Staggered Grid Computation of Fluid Flow with an Improved Discretisation of Finite Differencing

Nursalasawati Rusli[1,2], Ahmad Beng Hong Kueh[2], and Erwan Hafizi Kasiman[2]

[1] Institute of Engineering Mathematics, Universiti Malaysia Perlis,
02000 Kuala Perlis, Perlis, Malaysia
[2] Steel Technology Centre, Faculty of Civil Engineering,
Universiti Teknologi Malaysia, 81310 Skudai, Johor, Malaysia
nursalasawati@unimap.edu.my, {kbhahmad,erwanhafizi}@utm.my

Abstract. The present paper models the fundamental problems of fluid flow using a discretely improved finite difference method on a staggered computational grid. The developed finite difference formulation is applied to well-established benchmark problems, namely, the lid-driven cavity flow, the developing laminar flow in a straight rectangular duct and the backward-facing step flow. Excellent agreements have been found for all cases. Also, this approach has successfully handled the pressure of the flow that has been long considered as one of the main problems in using the finite difference method.

Keywords: finite difference method, Navier-Stokes equations, incompressible flow, staggered grid.

1 Introduction

Over the past few decades, numerical modelling of fluid flow has been a major topic of research in modern science and engineering [1]. Computational fluid dynamics (CFD) occupies one of the key physical disciplines that involve the description of fluid flow in terms of mathematical models which comprise convective and diffusive transports of matters. Basically, it constitutes the groundwork covering the fields of mechanical engineering, marine engineering, aeronautics and astronautics, civil engineering and bioengineering, to name a few. Inherent in the core of fluid flow study are the mathematical models that consist of a set of governing equations in the form of ordinary or partial differential equations. Although a great account of analytical solutions for CFD is available, in practical applications, it is customary to resolve the solutions in numerical form. One of the chief techniques frequently used in the investigation of CFD is the finite difference method (FDM).

In obtaining solutions for CFD problems, one of the main concerns of the FDM is the handling of the pressure of the flow. In general, physical specification of pressure is absent, as it is implicitly correlated to the problem description. Even though there are three equations for the three unknowns u, v, p, there is no explicit equation which can be used for pressure. In most finite difference solution schemes for incompressible steady flows, the pressure field is obtained from a Poisson equation which is derived

A. Abd Manaf et al. (Eds.): ICIEIS 2011, Part III, CCIS 253, pp. 82–94, 2011.

from the momentum equations and the continuity equation [2]. The difficulty inherited from this approach is the need to decide on additional boundary conditions on the pressure [3]. This problem has been discussed in details in [4].

To overcome this issue, [5] recently presented a point based compact finite difference method on a staggered grid, using a fully explicit second-order accurate time marching scheme, where the pressure Poisson equation is solved by a pseudo-time marching procedure. Elsewhere, a new scheme that is implemented with the SIMPLE-type algorithm for the pressure field calculation similar to that of finite volume methods was proposed by [6] to solve this problem. The discretised equations are developed as a purely finite difference formulation. The convective terms in the momentum equations are approximated using the first or second order finite difference formulae. [6] used unequally spaced grid points for handling *u*- and *v*-momentum equations at a wall boundary, whereas an equally spaced grid points are chosen in this study for the same nodes.

The present work concerns with the formulation of the scheme and the validation of the benchmark problems based on the improved model. First, the governing equations are presented in Section 2. Then, section 3 discusses the new scheme in details. Finally, section 4 presents the validation of this method and its analysis.

2 Governing Equations

In the current study, we shall be interested in the standard Navier-Stokes governing equations and continuity of incompressible fluid flow given as follows

continuity equation

$$\frac{\partial u^*}{\partial x^*} + \frac{\partial v^*}{\partial y^*} = 0 \tag{1}$$

x-momentum equation

$$u^* \frac{\partial u^*}{\partial x^*} + v^* \frac{\partial u^*}{\partial y^*} = -\frac{1}{\rho}\frac{\partial p^*}{\partial x^*} + \nu\left(\frac{\partial^2 u^*}{\partial x^{*2}} + \frac{\partial^2 u^*}{\partial y^{*2}}\right) \tag{2}$$

y-momentum equation

$$u^* \frac{\partial v^*}{\partial x^*} + v^* \frac{\partial v^*}{\partial y^*} = -\frac{1}{\rho}\frac{\partial p^*}{\partial y^*} + \nu\left(\frac{\partial^2 v^*}{\partial x^{*2}} + \frac{\partial^2 v^*}{\partial y^{*2}}\right) \tag{3}$$

where u and v are the velocity components in the x and y directions respectively, p is the pressure, ρ is the constant density, and ν is the viscosity.

Using the dimensionless definitions as given by [7], the governing equations (1) to (3) become

$$\frac{\partial u}{\partial x}+\frac{\partial v}{\partial y}=0 \tag{4}$$

$$u\frac{\partial u}{\partial x}+v\frac{\partial u}{\partial y}=-\frac{\partial p}{\partial x}+\frac{1}{\mathrm{Re}}\left(\frac{\partial^2 u}{\partial x^2}+\frac{\partial^2 u}{\partial y^2}\right) \tag{5}$$

$$u\frac{\partial v}{\partial x}+v\frac{\partial v}{\partial y}=-\frac{\partial p}{\partial y}+\frac{1}{\mathrm{Re}}\left(\frac{\partial^2 v}{\partial x^2}+\frac{\partial^2 v}{\partial y^2}\right) \tag{6}$$

where $\mathrm{Re}=\dfrac{Uh}{\nu}$ is the Reynolds number.

3 Numerical Method

The governing equations presented in the previous section are solved using a new numerical algorithm proposed by [6]. The methodology is finite difference based, but essentially takes advantage of the best features of two well-established numerical formulations, the finite difference and the finite volume methods. Some weaknesses of the finite difference approach are removed by exploiting the strengths of the finite volume method.

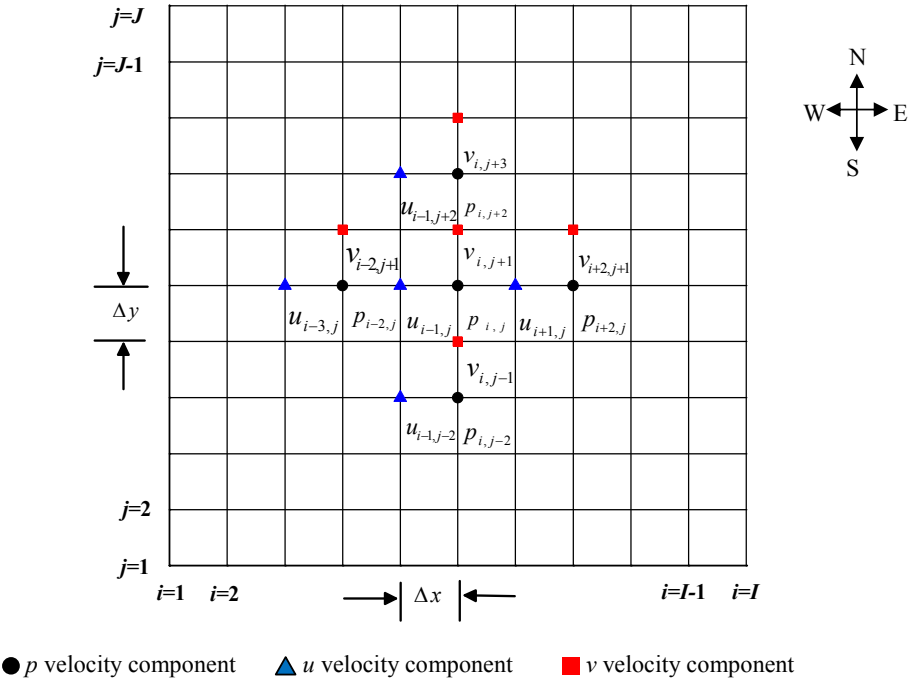

Fig. 1. Staggered grid arrangement

3.1 Finite Differencing on a Staggered Grid

We shall proceed next by considering a two-dimensional rectangular cavity flow domain which is subdivided using a regular Cartesian mesh as demonstrated in Figure 1. The mesh is evenly distributed in *x* and *y* directions. Here, a staggered grid is used to store the velocity components *u* and *v* and the pressure *p*.

We can see in Figure 1 that the values of *u* and *v* are stored at the *i-1,j* and *i,j+1* locations respectively and *p* is stored at *i,j*. A direct indication of such an arrangement is that the *u*-momentum (equation 5) is discretised at *i-1,j*, the *v*-momentum (equation 6) at *i,j+1*, and the continuity (equation 1) at *i,j*. Here, a first-order upwind differencing scheme has been employed to approximate the convective terms in the momentum equations, while a second-order central differencing is adopted for the diffusion terms. The pressure gradients are approximated by a second order central difference scheme.

3.2 Discretisation of the Momentum Equations

Unequally spaced grid points have been subscripted for the handling of *u*- and *v*-momentum equations at the wall boundary in [6]. As a result, the convective term is approximated using a second order accurate expression while the diffusion term takes the first order accurate expression, both of which lead to the formation of different formulae at different node location. For convenience, equally spaced grid points are chosen in this study. The advantage here is that the discretisation of the *u*- and *v*-momentum equations at interior nodes can be used at the wall boundary. To demonstrate the scheme, the discretisation of the momentum equations is summarized as below.

3.2.1 *u*-Momentum Equation

The discrete *u*-momentum equations at interior nodes are given by

$$a_P^{\text{int}} u_{i-1,j} + a_N^{\text{int}} u_{i-1,j+2} + a_S^{\text{int}} u_{i-1,j-2} + a_W^{\text{int}} u_{i-3,j} + a_E^{\text{int}} u_{i+1,j} = \frac{\hat{p}_{i-2,j} - \hat{p}_{i,j}}{2\rho\Delta x}$$

where

$$a_P^{\text{int}} = \frac{\hat{u}_{i-1,j}}{2\Delta x} + \nu\left(\frac{1}{2\Delta x^2} + \frac{1}{2\Delta y^2}\right)$$

$$a_N^{\text{int}} = \frac{\hat{v}_{i-1,j}}{4\Delta y} - \frac{\nu}{4\Delta y^2}$$

$$a_S^{\text{int}} = -\frac{\hat{v}_{i-1,j}}{4\Delta y} - \frac{\nu}{4\Delta y^2}$$

$$a_W^{\text{int}} = -\frac{\hat{u}_{i-1,j}}{2\Delta x} - \frac{\nu}{4\Delta x^2}$$

$$a_E^{\text{int}} = -\frac{\nu}{4\Delta x^2}$$

It shall be pointed out that the variables with the carets above them are the quantities to be calculated at the previous iteration. Because of the use of a staggered grid, the values of v in the u-momentum equation and u in the v-momentum equation, appearing as the coefficients of the convective derivatives, are not available at the desired points.

Consequently, these velocities are computed to a second order accuracy using the velocities of four surrounding grid points described as the followings,

$$u\big|_{i,j+1} = \frac{u_{i+1,j} + u_{i+1,j+2} + u_{i-1,j} + u_{i-1,j+2}}{4}$$

$$v\big|_{i-1,j} = \frac{v_{i,j-1} + v_{i,j+1} + v_{i-2,j-1} + v_{i-2,j+1}}{4}$$

Additional modifications have been made for the discrete u-momentum equations of interior nodes which are otherwise identical to those of boundary nodes. For example, the discrete u-momentum equations at the inlet nodes is the same as interior node except that the value of $u_{1,j}$ is known.

The u-momentum equation along the bottom of the wall $(j=2)$ takes the form

$$a_P^S u_{i-1,2} + a_N^S u_{i-1,4} + a_W^S u_{i-3,2} + a_E^S u_{i+1,2} = \frac{\hat{p}_{i-2,2} - \hat{p}_{i,2}}{2\rho\Delta x} + \left(\frac{2\nu}{3\Delta y^2} + \frac{2v_{i-1,2}}{3\Delta y}\right) u_{i-1,1}$$

where

$$a_P^S = \frac{\hat{u}_{i-1,2}}{2\Delta x} + \frac{\hat{v}_{i-1,2}}{2\Delta y} + \nu\left(\frac{1}{2\Delta x^2} + \frac{1}{2\Delta y^2}\right)$$

$$a_N^S = \frac{\hat{v}_{i-1,2}}{6\Delta y} - \frac{\nu}{3\Delta y^2}$$

$$a_W^S = -\frac{\hat{u}_{i-1,2}}{2\Delta x} - \frac{\nu}{4\Delta x^2}$$

$$a_E^S = -\frac{\nu}{4\Delta x^2}.$$

In a refined form, the current method presents the u-momentum equation along the bottom of the wall as

$$a_P^{\text{int}} u_{i-1,2} + a_N^{\text{int}} u_{i-1,4} + a_W^{\text{int}} u_{i-3,2} + a_E^{\text{int}} u_{i+1,2} = \frac{\hat{p}_{i-2,2} - \hat{p}_{i,2}}{2\rho\Delta x} - a_S^{\text{int}} u_{i-1,1}$$

Here, all other coefficients are the same as defined at the interior nodes.

3.2.2 v-Momentum Equation

Similar to the discrete u-momentum equations, the discrete v-momentum equations at the interior nodes take the following form

$$b_P^{\text{int}} v_{i,j+1} + b_N^{\text{int}} v_{i,j+3} + b_S^{\text{int}} v_{i,j-1} + b_W^{\text{int}} v_{i-2,j+1} + b_E^{\text{int}} v_{i+2,j+1} = \frac{\hat{p}_{i,j} - \hat{p}_{i,j+2}}{2\rho\Delta y}$$

where

$$b_P^{\text{int}} = \frac{\hat{u}_{i,j+1}}{2\Delta x} + \nu\left(\frac{1}{2\Delta x^2} + \frac{1}{2\Delta y^2}\right)$$

$$b_N^{\text{int}} = \frac{\hat{v}_{i,j+1}}{4\Delta y} - \frac{\nu}{4\Delta y^2}$$

$$b_S^{\text{int}} = -\frac{\hat{v}_{i,j+1}}{4\Delta y} - \frac{\nu}{4\Delta y^2}$$

$$b_W^{\text{int}} = -\frac{\hat{u}_{i,j+1}}{2\Delta x} - \frac{\nu}{4\Delta x^2}$$

$$b_E^{\text{int}} = -\frac{\nu}{4\Delta x^2}\,.$$

3.3 Discretisation of the Continuity Equation

For present model, the pressure correction equations that are identical to those given in [6] are employed for all boundary nodes. The pressure correction equations for the interior nodes are

$$c_P^{\text{int}} p'_{i,j} + c_E^{\text{int}} p'_{i+2,j} + c_W^{\text{int}} p'_{i-2,j} + c_N^{\text{int}} p'_{i,j+2} + c_S^{\text{int}} p'_{i,j-2} = \frac{u^{*'}_{i-1,j} - u^{*}_{i+1,j}}{2\Delta x} - \frac{v^{*'}_{i,j+1} - v^{*}_{i,j-1}}{2\Delta y}$$

where

$$c_P^{\text{int}} = \frac{1}{4\rho\Delta x^2 a_{i+1,j}} + \frac{1}{4\rho\Delta x^2 a_{i-1,j}} + \frac{1}{4\rho\Delta y^2 b_{i,j+1}} + \frac{1}{4\rho\Delta y^2 b_{i,j-1}}$$

$$c_E^{\text{int}} = -\frac{1}{4\rho\Delta x^2 a_{i+1,j}}$$

$$c_W^{\text{int}} = -\frac{1}{4\rho\Delta x^2 a_{i-1,j}}$$

$$c_N^{\text{int}} = -\frac{1}{4\rho\Delta y^2 b_{i,j+1}}$$

$$c_S^{\text{int}} = -\frac{1}{4\rho\Delta y^2 b_{i,j-1}}$$

3.4 Solution Algorithm

For convenience, we customarily use the SIMPLE scheme for the pressure-velocity coupling in the overall solution. The numerical algorithm for one complete cycle is given in the flow chart below.

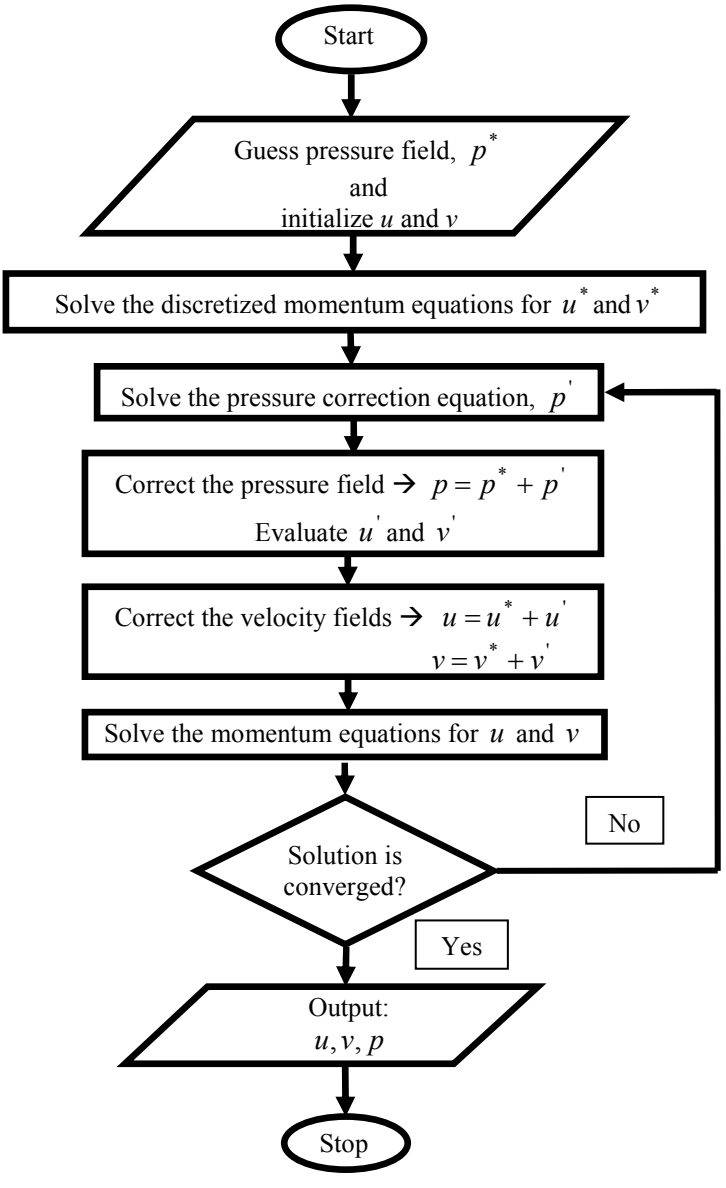

Fig. 2. Flow chart for the SIMPLE-type algorithm

It shall be stressed that the pressure-correction equation is prone to diverge from desired solution path unless an under-relaxation is implemented. For such a purpose, the following is used.

$$p = p^{*} + \alpha_P p'$$

where α_P is the pressure under-relaxation parameter. Due to expensive computational time in achieving convergence, the Tri-Diagonal Matrix Algorithm (TDMA) used by [6] to solve the system of discretised equations is avoided. In the present algorithm, a modification is provided in the form of a direct method to remedy such a problem. It has been shown that a rapid convergence can be obtained through this method [8].

4 Test Problem

To measure the validity of current model, the developed finite difference formulation is used to simulate the well-established benchmark problems. In the following sections, we shall be interested in the comparison of currently modeled solution to those of classical problems, namely, the lid-driven cavity flow, the developing laminar flow in a straight rectangular duct and the backward-facing step flow. Note the comparisons are restricted to those of low Re numbers. Turbulent flow is not considered in the current study.

4.1 Lid-Driven Cavity Flow

The lid-driven cavity problem has long been considered as the test or validation case for new codes or new solution methods. Among the reasons for such popularity are the problem geometry is simple and two-dimensional. Furthermore, the boundary conditions are considerably simple. The standard case is fluid contained in a square domain with the Dirichlet boundary conditions on all sides, with three stationary sides and one moving side (with a prescribed velocity tangent to the side). The boundary conditions for the present problem are illustrated in Figure 3.

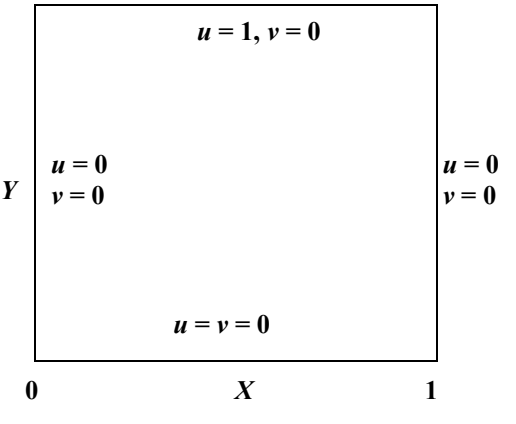

Fig. 3. Boundary conditions for the lid-driven cavity

Since this problem case has been solved and used frequently for verification, there exists a great deal of data to compare with. A good set of data for comparison is the data given in [1]. It includes tabulated results for various Reynolds numbers.

In the comparison, we shall consider the flow for aforementioned problem for $\mathrm{Re} = 100$. Figure 4(a) illustrates the velocity component u along the vertical line through the geometric centre of cavity. Figure 4(b) shows the velocity component v along the horizontal line through the geometric centre of cavity. Obviously, one can see in the figures that very good agreements are demonstrated from the comparison of the present model with those obtained by [1] and [6].

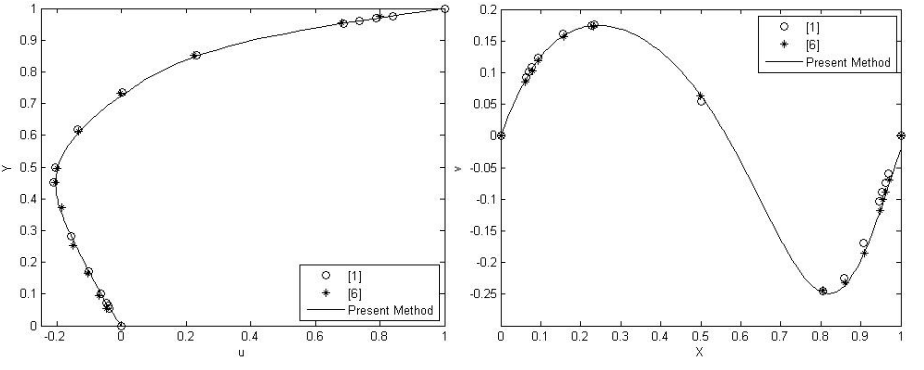

(a) Vertical (b) Horizontal

Fig. 4. Velocity along the vertical and horizontal lines through the geometric centre of cavity for $\mathrm{Re} = 100$

The velocity vector plot and contour for $\mathrm{Re} = 100$ are shown in Figure 5. One can see that the features of the cavity flow are excellently captured.

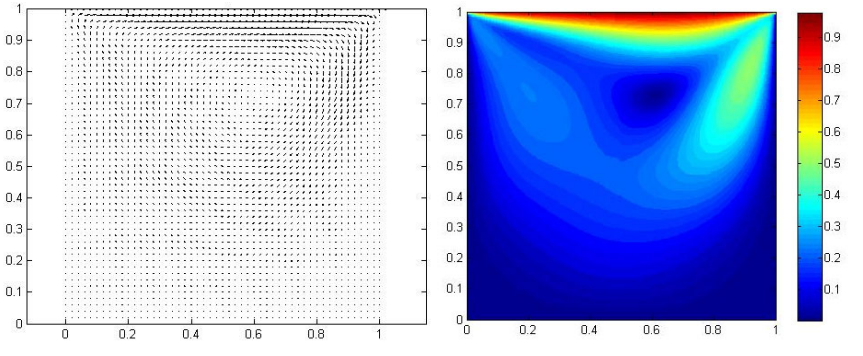

(a) Velocity plot (b) velocity contour

Fig. 5. Velocity plot and contour of the cavity flow for $\mathrm{Re} = 100$

4.2 Developing Flow in a Rectangular Duct

Next, consider a developing flow in a straight two-dimensional channel as shown in Figure 6. The length L of the channel is taken to be ten times the width D, and we take $D = 1$.

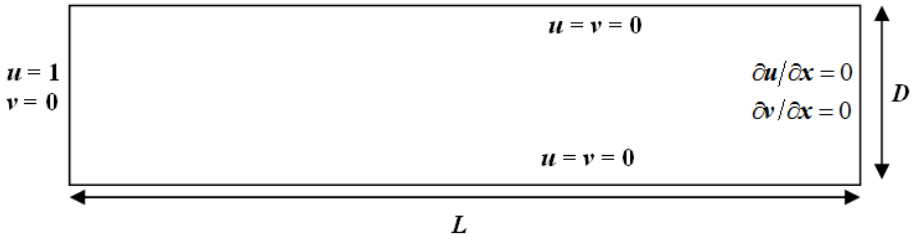

Fig. 6. Geometry of the channel with the prescribed boundary conditions

At the entrance of the channel, a uniform flow $(u = 1)$ is specified as the inlet velocity profile. The transverse velocity is set equal to zero at the inlet. A parallel flow condition is specified at the outlet, i.e. $\partial u/\partial x = 0$ and $\partial v/\partial x = 0$. The no-slip condition is applied at the lower and upper walls. As the fluid enters the channel, the wall boundary conditions distort the uniform flow due to the growth of boundary layers on the walls. The flow develops along the channel for some distance, until it becomes fully developed. At this point, the flow field is that described by the Poiseuille flow.

The numerical model is verified against the exact solution and Zogheib model for a fully developed flow formed at the outlet. Also, the predicted fully developed streamwise velocity profile for $\mathrm{Re} = 50$ is compared and the agreement is excellent, as given in Figure 7. In Figure 8, the result obtained for the present method closely matches the result from [6] and the agreement is better than that obtained from [9] where the parabolic profile of [9] starts further downstream, around $x = 4$. Velocity contour of the channel flow can be seen in Figure 9. Again, one can notice that it is considerably consistent with the behavior of the benchmark case (the latter is not shown here).

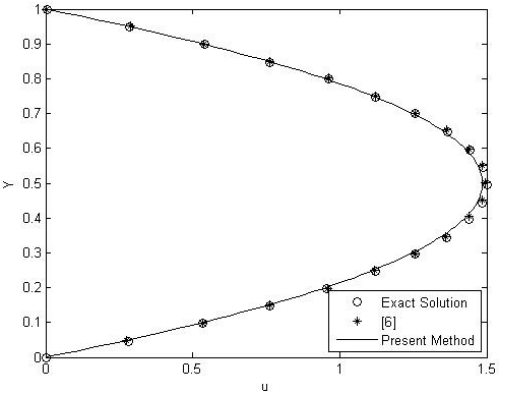

Fig. 7. Fully developed velocity profile

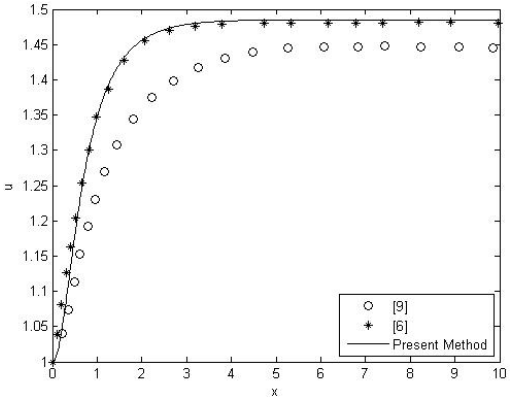

Fig. 8. Centreline velocity for $\mathrm{Re} = 50$

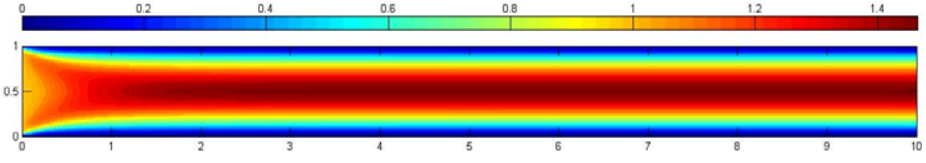

Fig. 9. Velocity contour of the flow

4.3 Backward-Facing Step Flow

The backward-facing step is one of the most fundamental geometries causing flow separation and is an important validation test for any numerical model.

Sketch of the geometry and boundary conditions for backward-facing step flow model is illustrated in Figure 10. The channel was defined to have height $2h$, with a step height and upstream inlet equal to h. In this work, we have taken $2h = 1$. The length L from the step to the end of the channel domain depends on Re. This length must be chosen to ensure the reattachment length is independent of the length of the calculation domain. Figure 11 shows the development of flow velocity vector in the channel.

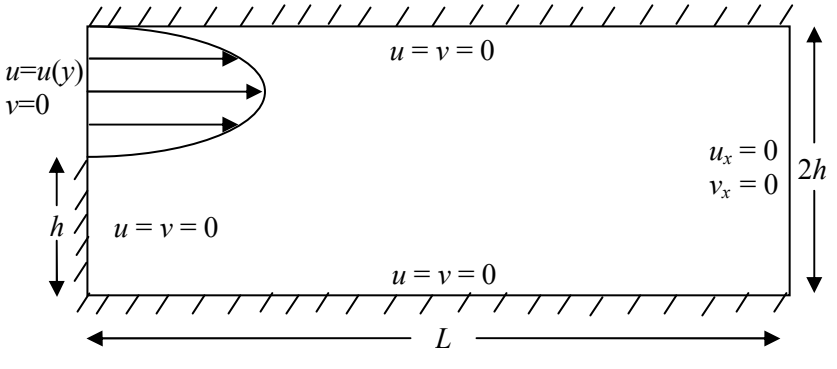

Fig. 10. Sketch of geometry for backward-facing step flow

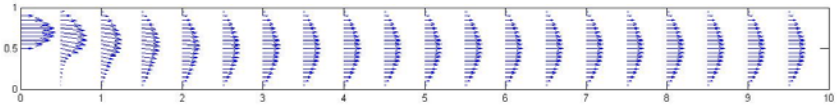

Fig. 11. Velocity plot of the flow

Table 12 gives a comparison of the reattachment length predicted by the present method with experimental and numerical results of [10] and [11]. It is clear that the computed results agree very well with those found in the literature.

Re	[10] (Experimental)	[11] (Numerical)	Present method (Numerical)
50	0.90	1.00	1.00
100	1.40	1.50	1.50
200	2.50	2.60	2.00

Fig. 12. Reattachment length as a function of Re

For demonstration purpose, we show next the contour and streamline plots for the channel for Re = 50 and Re = 100, respectively in Figures 13 and 14. It is obvious that an increase in Re boosts the velocity of flow especially near the entrance of channel. Nevertheless, the streamline plots display practically identical pattern for both flows.

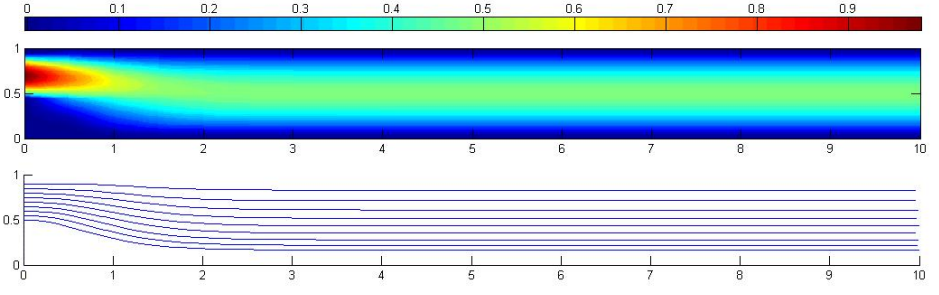

Fig. 13. *u* velocity contour and streamlines for Re=50

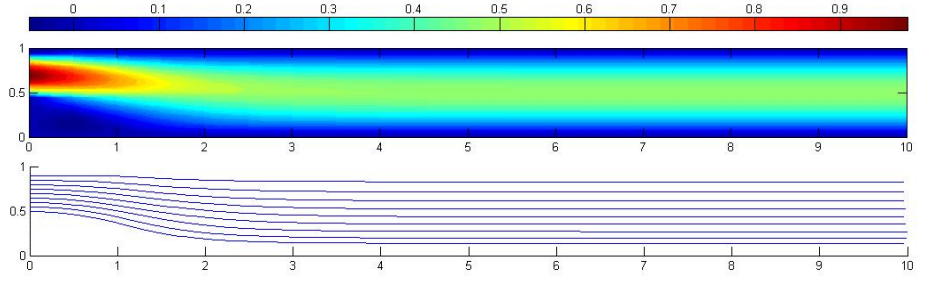

Fig. 14. *u* velocity contour and streamlines for Re=100

5 Conclusions

An improved finite difference discretisation method for solving the two-dimensional, steady, incompressible, laminar, viscous flow equations on a staggered grid is presented. The validation is done for the fundamental fluid flow problems, namely, the lid-driven cavity flow, the developing laminar flow in a straight rectangular duct and the backward-facing step flow. Good agreements are demonstrated by the current model with respect to these benchmark tests.

References

1. Ghia, U., Ghia, K.N., Shin, C.T.: High-Re Solutions for Incompressible Flow Using the Navier-Stokes Equations and a Multigrid Method. Journal of Computational Physics 48, 387–411 (1982)
2. Johnston, H., Liu, J.G.: Finite Difference Schemes for Incompressible Flow Based on Local Pressure Boundary Condition. Journal of Computational Physics 180, 120–154 (2002)
3. Strikwerda, J.C.: High Order-accurate Schemes for Incompressible Viscous Flow. International Journal for Numerical Methods in Fluids 24, 715–734 (1997)
4. Petersson, N.A.: Stability of Pressure Boundary Conditions for Stokes and Navier-Stokes Equations. Journal of Computational Physics 172, 40–70 (2001)
5. Zhang, K.K.Q., Shotorban, B., Minkowycz, W.J., Mashayek, F.A.: Compact Finite Difference Method on Staggered Grid for Navier–Stokes Flows. International Journal for Numerical Methods in Fluids 52, 867–881 (2006)
6. Zogheib, B.: Velocity-Pressure Coupling in Finite Difference Formulations for the Navier-Stokes Equations, Windsor, Ontario, Canada (2006)
7. Midya, C., Layek, G.C., Gupta, A.S., Mahapatra, T.R.: Magnetohydrodynamic Viscous Flow Separated in a Channel With Constrictions. Journal of Fluid Engineering 125, 952–962 (2003)
8. Ferziger, J.H., Peric, M.: Computational Methods for Fluid Dynamics, 3rd edn. Springer, USA (2002)
9. Reggio, M., Camarero, R.: Numerical Solution Procedure for Viscous Incompressible Flows. Numerical Heat Transfer 10, 131–146 (1986)
10. Armaly, B.F., Durst, F., Pereira, J.C.F., Schonung, B.: Experimental and Theoretical Investigation of Backward-facing Step Flow. Journal of Fluid Mechanics 127, 473–496 (1983)
11. Barber, R.W., Fonty, A.: Comparison of Vortex-element and Finite-volume Simulations of Low Reynolds Number Flow over a Confined Backward Facing Step. In: Proceedings of 11th Annual Conference of the CFD Society of Canada, CFD 2003, vol. 2, pp. 780–787 (2003)